Journal of Molecular Modeling (2019) 25: 328
https://doi.org/10.1007/s00894-019-4196-z

ORIGINAL PAPER

Identification of potent L,D-transpeptidase 5 inhibitors for *Mycobacterium tuberculosis* as potential anti-TB leads: virtual screening and molecular dynamics simulations

Victor T. Sabe[1] · Gideon F. Tolufashe[1] · Collins U. Ibeji[1] · Sibusiso B. Maseko[1] · Thavendran Govender[1] · Glenn E. M. Maguire[1,2] · Gyanu Lamichhane[3] · Bahareh Honarparvar[1] · Hendrik G. Kruger[1]

Received: 5 October 2018 / Accepted: 28 August 2019 / Published online: 28 October 2019

Abstract

Virtual screening is a useful in silico approach to identify potential leads against various targets. It is known that carbapenems (doripenem and faropenem) do not show any reasonable inhibitory activities against L,D-transpeptidase 5 (Ldt_{Mt5}) and also an adduct of meropenem exhibited slow acylation. Since these drugs are active against L,D-transpeptidase 2 (Ldt_{Mt2}), understanding the differences between these two enzymes is essential. In this study, a ligand-based virtual screening of 12,766 compounds followed by molecular dynamics (MD) simulations was applied to identify potential leads against Ldt_{Mt5}. To further validate the obtained virtual screening ranking for Ldt_{Mt5}, we screened the same libraries of compounds against Ldt_{Mt2} which had more experimetal and calculated binding energies reported. The observed consistency between the binding affinities of Ldt_{Mt2} validates the obtained virtual screening binding scores for Ldt_{Mt5}. We subjected 37 compounds with docking scores ranging from − 7.2 to − 9.9 kcal mol^{-1} obtained from virtual screening for further MD analysis. A set of compounds ($n = 12$) from four antibiotic classes with ≤ − 30 kcal mol^{-1} molecular mechanics/generalized born surface area (MM-GBSA) binding free energies (ΔG_{bind}) was characterized. A final set of that, all β-lactams ($n = 4$), was considered. The outcome of this study provides insight into the design of potential novel leads for Ldt_{Mt5}.

Keywords Virtual screening · Molecular dynamics (MD) · *Mycobacterium tuberculosis* (*M.tb*) · L,D-transpeptidase 5 (Ldt_{Mt5}) · Molecular mechanics/generalized born surface area (MM-GBSA)

Introduction

The alarming rise of multi and extensively drug-resistant tuberculosis (TB) has become a serious global health threat [1]. The emergence of resistant strains is partly due to poor patient compliance to the extensive treatment regimen [2, 3]. Thus, the identification of new anti-TB leads, particularly Ldt_{Mt5}, that can shorten the treatment regimen and target the resistant TB strains is urgently needed. *Mycobacterium tuberculosis* possesses a peptidoglycan (PG) layer that encapsulates the cytoplasmic membrane and is essential for cellular growth and viability [4]. The peptidoglycan structure of *Mycobacterium tuberculosis* (*M.tb*) from a stationary-phase culture revealed a high content (80%) of non-classical 3 → 3 cross-links generated by L,D-transpeptidation [5]. The classical 4 → 3 cross-links are predominantly formed by the D,D-transpeptidation activity of penicillin-binding proteins (PBPs) during the exponential phase of growth [6–9]. L,D-transpeptidases (Ldts) and PBPs are structurally

Electronic supplementary material The online version of this article (https://doi.org/10.1007/s00894-019-4196-z) contains supplementary material, which is available to authorized users.

✉ Bahareh Honarparvar
Honarparvarb@ukzn.ac.za

✉ Hendrik G. Kruger
kruger@ukzn.ac.za

[1] Catalysis and Peptide Research Unit, School of Health Sciences, University of KwaZulu-Natal, Durban 4001, South Africa

[2] School of Chemistry and Physics, University of KwaZulu-Natal, Durban 4001, South Africa

[3] Center for Tuberculosis Research, Division of Infectious Diseases, School of Medicine, Johns Hopkins University, Baltimore, MD 21205, USA

similar [10] and contain the catalytic active sites with cysteine and serine residues, respectively [11]. Five Ldt paralogues have been identified for *M.tb*, Ldt_{Mt1}, to Ldt_{Mt5}. Reported experimental and theoretical studies revealed that both Ldt_{Mt1} and Ldt_{Mt2} can be inactivated by carbapenems, a class of β-lactam antibiotics [5, 6, 8, 12, 13]. These two enzymes, also have distinct functions in vivo [5, 9]. It has been shown that Ldt_{Mt1} may have a role in adaptation to the non-replicative state of the bacilli [5], while Ldt_{Mt2} is essential for virulence in a mouse model of acute infection [9]. For *M.tb*, Ldt_{Mt5} is required for properly maintaining cell wall integrity [4] and a more recent study also revealed that four L,D paralogues, with the exception of Ldt_{Mt3}, are active in in vitro peptidoglycan cross-linking assays, and that all but Ldt_{Mt5} are inhibited by carbapenems [7].

The single crystal X-ray structure of the extra-cellular portion of Ldt_{Mt5} was recently published [4]. Modest enhancement in susceptibility of *M.tb* to certain carbapenems (doripenem and faropenem) was observed presumably due to synthetic lethality, as these β-lactams may inactivate other targets. Meanwhile, a meropenem-adduct crystal structure was reported which supports the idea that very slow acylation of Ldt_{Mt5} occurs over many days. The structures of apo-Ldt_{Mt5} and its meropenem-Ldt_{Mt5} adduct (Fig. 1) demonstrate that, despite the overall structural similarity to Ldt_{Mt2}, the Ldt_{Mt5} active site residues are different [4].

The presence of a structurally divergent catalytic site and a proline-rich C-terminal subdomain suggests that this protein may have a distinct role in PG metabolism, perhaps involving other cell wall–anchored proteins. Also, *M.tb* lacking a functional copy of Ldt_{Mt5} displays aberrant growth and is more susceptible to killing by osmotic shock, select carbapenem antibiotics and crystal violet [4]. The β-lactam and oxazolidinone compounds will most likely be able to form covalent bonds with the catalytic cysteine of Ldt_{Mt5} probably due to the carbonyl and amide functional group in the structural backbone. Hence, in case any promising inhibitors from the other classes are identified, they will most likely act as competitive [14] inhibitors.

Carbapenems gave insignificant binding of Ldt_{Mt5} experimentally using isothermal titration calorimetry (ITC). Carbapenems are considered the last-resort antibiotics to treat resistant bacterial infections in humans [15–23]. This fact motivated us to perform a virtual screening of five classes of known TB antibiotics (Fig. 1). Virtual screening with both AutoDock Vina and Schrödinger Maestro software programs was performed as a benchmark for the automated docking. Molecular dynamics and binding free energy studies were performed on each of the screened compounds from the five classes of anti-TB agents. To the best of

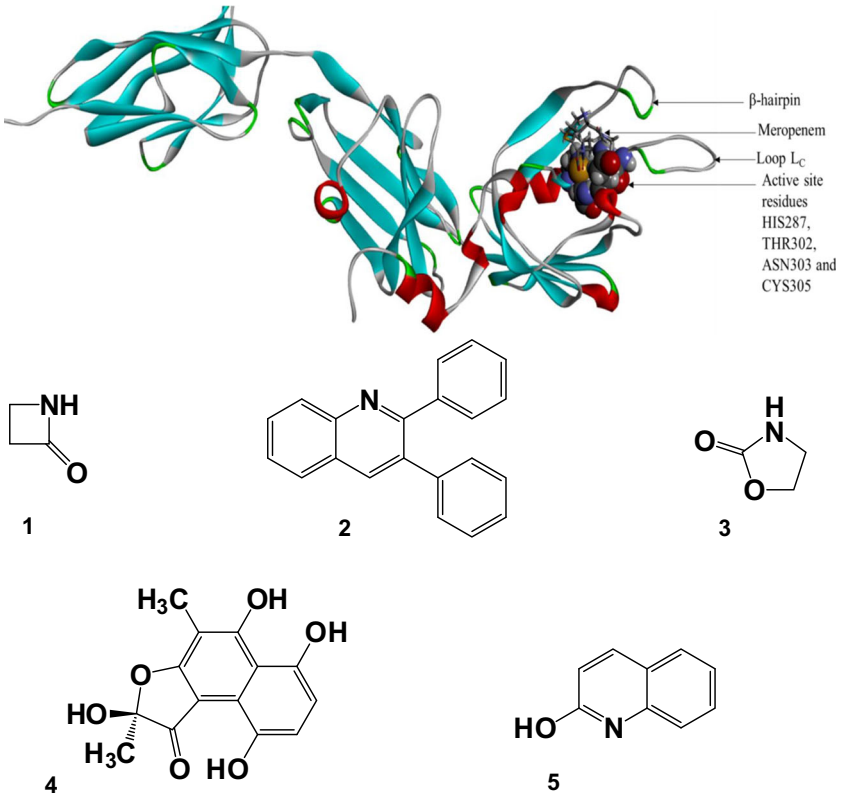

Fig. 1 The rendering of MERO-Ldt_{Mt5} crystal X-ray structure (PDB code: 4ZFQ). Shown is a β-hairpin flap (312–330), Lc loop (338–358) and active site pocket in CPK form [HIS287 (342), THR302 (357), ASN303 (358), and CYS305 (360)] and meropenem (inhibitor) in stick form [4] (top) and the 2D scaffold structures of (1) β-lactam, (2) diarylquinoline, (3) oxazolidinone, (4) rifamycin, and (5) quinolone classes of TB antibiotics (bottom)

Table 1 Parameters set for all screened compounds which were subjected to Lipinski's rules and Veber's drug-like filter

Parameter	Minimum	Maximum
Molecular weight (g/mol)	32	500
xlogP	− 4.00	5
Net charge	− 5	5
Rotatable bonds	0	10
Polar surface area (Å^2)	0	140
Hydrogen donors	0	5
Hydrogen acceptors	0	10
Polar solvation (kcal mol^{-1})	− 400	1
Apolar solvation (kcal mol^{-1})	− 100	40

our knowledge, a computational model to identify and rank the different anti-TB agents against Ldt_{Mt5} has not yet been reported.

Materials and methods

The following in silico approaches were used to screen five classes of known TB antibiotics (Fig. 1) against Ldt_{Mt5}. The automated docking process was performed using Autodock Vina [24] and Schrödinger Maestro [25] programs which implement the quasi-flexible docking method to perform the screening [26]. The docked energies followed by visual inspection of the inhibitor pose were performed to ensure the close proximity of the selected compounds with the catalytic cysteine. This was followed by molecular dynamics simulations/MD trajectory analyses using CPPTRAJ module [27] implemented in Amber 14 [28] package on GPU-accelerated PMEMD engine.

System preparation

The 3D crystal structure of the meropenem-bound Ldt_{Mt5} (PDB code: 4ZFQ [4]) was retrieved from the Protein Data Bank [29]. The missing residues (the β-hairpin flap is missing having the loop LC and the ex-CTSD being disordered) [4] of the Ldt_{Mt5} enzyme were refined using MODELLER v9.15 [30]. Assignment of the protonation states of the enzyme residues at pH = 7 was performed by recalculating the standard pKa values of the titratable amino acids using the empirical propKa server [31], similar to a study on Ldt_{Mt2} [32]. These protonation states of the titratable residues were used for the virtual screening and for the subsequent modelling.

The chemical compounds used for the screening were retrieved from the ZINC [33] database. This database is available for free download (http://zinc.docking.org) in different formats usable for computational studies [33]. Compounds from five classes of known TB antibiotics were subjected for the initial screening based on their mode of action. Each scaffold of the five classes was drawn using the 2D Sketcher tool implemented in ZINC GUI. A structural similarity index of 99% was set for all compounds except for rifamycin in which ligand mining could only be performed at a similarity index of 50%. All the screened compounds obeyed Lipinski's rule [34] of drug-likeness to filter the compound molecules and Veber's criteria for oral bioavailability of drug candidates [35]. The considered Lipinski's parameters [34] are as follows: molecular weight; xlogP; net charge; rotatable bonds; polar surface area; hydrogen donors; hydrogen acceptors; and polar and apolar solvation (Table 1).

Virtual screening using AutoDock Vina

AutoDock Vina is a program for molecular docking and virtual screening. The prepared 3D structure of Ldt_{Mt5} [4] in PDB format was converted to pdbqt format using raccoon [24], likewise the library of compounds downloaded from ZINC database in mol2 format was converted to pdbqt format. Virtual screening using automated docking involves the preparation of the receptor (this includes assigning of Kollman charges [36] and Gasteiger partial charges [37] to all atoms and assignment of AD4 types to atoms of the protein structure), ligands and a config file in which grid center, a grid box size, and a docking run number are assigned. AutoDock tools 1.5.6 [38] were employed to determine the proper size of the grid box for the potential binding site for the lead compounds and the receptor grid center was set on Cys305 (360) (active site reactive residue) [4]. The grid box was determined as the center ($X = 3.9$, $Y = -39.5$, $Z = 12.1$) and dimension ($X = 45$, $Y = 45$, $Z = 45$) with the grid spacing of 0.375 Å were

Table 2 The selected five categories of antibacterial compounds from ZINC database

Class	Mode of action	Number of screened compounds
β-lactam	Cell wall biosynthesis (inhibition of transpeptidase and inhibition of β-lactamase by clavulanic acid)	2707
Diarylquinoline	ATP synthesis inhibition (subunit c of ATP synthase)	4309
Oxazolidinone	Protein synthesis inhibition	3065
Rifamycin	RNA synthesis inhibition (inhibition of RNA polymerase)	2678
Quinolone	DNA synthesis inhibition (inhibition of gyrase)	7

Table 3 The top 10 ligands per class based on the lowest docked energies were chosen for AutoDock Vina against Ldt_{Mt5} (The optimal ligands in the active pocket, highlighted in blue, were selected for further MD analysis). The docked 3D structures (PDB format) for all the lead compounds in complex with Ldt_{Mt5} are provided as supplementary information

Antibiotic class	Ligand identity	Docking score (kcal mol^{-1})
β-lactam		
1	ZINC 01662030	− 8.4
2	ZINC 02475683	− 8.4
3	ZINC 02475684	− 8.4
4	ZINC 01662029	− 8.3
5	ZINC 02462884	− 8.3
6	ZINC 03791246	− 8.3
7	ZINC 01412853	− 8.3
8	ZINC 01385054	− 8.2
9	ZINC 01412838	− 8.2
10	ZINC 01412839	− 8.2
Rifamycin		
1	ZINC 19569373	− 8.6
2	ZINC 03197606	− 8.4
3	ZINC 14828615	− 8.4
4	ZINC 01551761	− 8.4
5	ZINC 13125731	− 8.2
6	ZINC 13125732	− 8.2
7	ZINC 14693083	− 8.2
8	ZINC 15216498	− 8.2
9	ZINC 33832153	− 8.2
10	ZINC 39227187	− 8.2
Oxazolidinone		
1	ZINC 03921583	− 8.7
2	ZINC 03921580	− 8.5
3	ZINC 00586642	− 8.4
4	ZINC 00003190	− 8.3
5	ZINC 00594969	− 8.3
6	ZINC 03785925	− 8.3
7	ZINC 03921504	− 8.3
8	ZINC 05774946	− 8.2
9	ZINC 03791902	− 8.2
10	ZINC 03921352	− 8.2
Diarylquinoline		
1	ZINC 00022457	− 9.0
2	ZINC 00022456	− 8.7
3	ZINC 00057310	− 8.2
4	ZINC 00075863	− 8.2
5	ZINC 00097351	− 8.2
6	ZINC 00152025	− 8.2
7	ZINC 00236246	− 8.1
8	ZINC 00254016	− 8.1
9	ZINC 00118842	− 8.0
10	ZINC 00192295	− 8.0
Quinolone		
1	ZINC 80595608	− 8.0
2	ZINC 80595598	− 7.9
3	ZINC 80595612	− 7.9
4	ZINC 78317542	− 7.6
5	ZINC 80595606	− 7.6
6	ZINC 79236395	− 7.4

AutoDock Vina top-ranked docking scores were considered, and the values are between − 7.4 and − 9.0 kcal mol^{-1}

considered for each of the following atom types: A, C, H, HD, N, OA, and SA representing all probable atom types in the target enzyme. Created, finally, was a conf.txt file which includes receptor in pdbqt format, a grid center with *x*, *y*, *z* coordinates, a grid box size in Å, and a docking run number of 10. The virtual screening was carried out using the python script, VS.bash executable on AutoDock Vina on Linux Ubuntu on a Dell CPU. Docked results were ranked based on the binding affinities and visual inspection to ensure an acceptable drug/enzyme interaction is present. Visual inspection of the selected ligands inside the enzyme was performed using the Discovery Studio [39] software program.

Virtual screening using Schrödinger Maestro

Schrödinger Maestro software program was applied for the docking studies. Protein/ligand preparation and virtual screening were all performed in the Maestro 11.2 graphical user interface [25]. The Protein Preparation Wizard [40] of the Schrödinger Maestro software program was used to prepare the 3D protein structure. The pre-processing of the protein was performed which includes assigning of bond orders; adding of hydrogens; creating zero-order bonds to metals; creating disulphide bonds; deleting crystallographic waters beyond 5.00 Å from hetero groups; and generating hetero states using Epik [41]: pH 7.0± 2.0. In the 3D protein structure refinement, the alignment of H-bonds was done using PROPKA pH 7.0 and waters with less than three hydrogen bonds to non-waters were removed. Restrained minimization was performed to converge heavy atoms to RMSD of 0.30 Å.

The 2D structures of the compounds were imported onto the Schrödinger Maestro project table and they were converted into a 3D model using the pre-set option. The LigPrep module [25] was used to refine the structures using default parameters. Ionization was performed to generate possible states at target pH 7.0± 2.0 using Epik [41] and tautomers were generated. The compounds were subjected to OPLS3 [42] (optimized potentials for liquid simulations) force field for energy optimization. For ligand preparation, the system was set to retain specified chiralities to 10 per ligand and the

Table 4 The Schrödinger Maestro top ligands per class based on the lowest Glide docking score against Ldt_{Mt5} (The optimal ligands in the active pocket, highlighted in blue, were selected for further MD analysis). The docked 3D structures (PDB format) for all the lead compounds in complex with Ldt_{Mt5} are provided as supplementary information

Antibiotic class	Ligand identity	Docking score (kcal mol^{-1})
β-lactam		
1	ZINC 03788344	− 9.9
2	ZINC 03788344	− 9.7
3	ZINC 03788344	− 9.4
4	ZINC 03788344	− 9.2
5	ZINC 03808350	− 8.8
6	ZINC 03788344	− 8.9
7	ZINC 03808351	− 8.7
8	ZINC 03808352	− 8.7
9	ZINC 03826440	− 8.4
10	ZINC 03826440	− 8.4
11	ZINC 03788344	− 8.4
12	ZINC 03785001	− 8.2
13	ZINC 03785029	− 8.2
14	ZINC 03808350	− 8.1
15	ZINC 03784242	− 7.9
Rifamycin		
1	ZINC 06483425	− 9.3
2	ZINC 06483423	− 9.3
3	ZINC 06483425	− 9.2
4	ZINC 06483423	− 9.2
5	ZINC 13532137	− 8.0
6	ZINC 59077219	− 7.9
7	ZINC 59077220	− 7.9
8	ZINC 59077221	− 7.9
9	ZINC 59077222	− 7.9
10	ZINC 59077219	− 7.9
11	ZINC 59077220	− 7.9
12	ZINC 59077221	− 7.9
Oxazolidinone		
1	ZINC 00108966	− 8.0
2	ZINC 00108966	− 8.0
3	ZINC 00108973	− 8.0
4	ZINC 00108973	− 8.0
5	ZINC 00108966	− 7.9
6	ZINC 00108966	− 7.9
7	ZINC 00108973	− 7.9
8	ZINC 00108973	− 7.9
9	ZINC 00052567	− 7.5
10	ZINC 00052568	− 7.5
11	ZINC 02512954	− 7.3
12	ZINC 02512954	− 7.2
13	ZINC 00108966	− 7.2
14	ZINC 00108966	− 7.2
Diarylquinoline		
1	ZINC 00096619	− 8.1
2	ZINC 00002447	− 7.7
3	ZINC 00002447	− 7.7
4	ZINC 00007109	− 7.5
5	ZINC 00060410	− 7.7
6	ZINC 00060410	− 7.7
7	ZINC 00060410	− 7.7
8	ZINC 00060410	− 7.7
9	ZINC 00060410	− 7.7
10	ZINC 00060410	− 7.7
Quinolone		
1	ZINC 80595598	− 3.6

Schrödinger Maestro top-ranked docking scores were considered, and the values are between − 7.2 and − 9.9 kcal mol^{-1}. The class Quinolone was eliminated for further MD analysis because of its low docking score of − 3.6 kcal mol^{-1}

output format was Maestro from Schrödinger software program. The grid box was positioned at the center and the receptor grid center was set on Cys305 (360) (active site reactive residue) [4] with grid spacing minimum distance of 1 Å and maximum distance of 3.5 Å. The *X*, *Y*, and *Z* coordinates were − 31.88, 23.5, and − 46.48 respectively. Default settings of Maestro 11.2 were used for other parameters such as constraints, rotatable groups, and sites.

Using a predetermined receptor grid, quasi-flexible docking [14, 26, 43] was performed via the Glide [44] mode of Schrödinger Maestro (Schrödinger, Inc). The system was set to resume post-docking minimization, setting the number of poses per ligand to 5. For filtering, default settings were employed and this includes applying the Epik state penalty parameters [25] for docking and the scaling of ligand van der Waals radii for non-polar atoms using the scaling factor 0.80 [45, 46] and partial charge cut-off 0.15 [45, 46]. Ligand docking was done using the three incremental stages of ranking accuracy, i.e., high-throughput virtual screening (HTVS), Glide simple precision (SP), and Glide extra precision (XP) [25]. The docking score (Glide GScore) from Glide extra precision (XP) was used to evaluate specific protein-ligand interactions within the active site of the enzyme.

The difference with these programs lies in the docking algorithm in which Schrödinger Maestro uses the Glide module which employs the Monte Carlo algorithm [47] that makes random moves and accepts or rejects each conformation based on Boltzmann probability while AutoDock Vina utilizes the AutoDock module. This program applies the genetic algorithm [48], which maintains a selective pressure towards an optimal solution, with

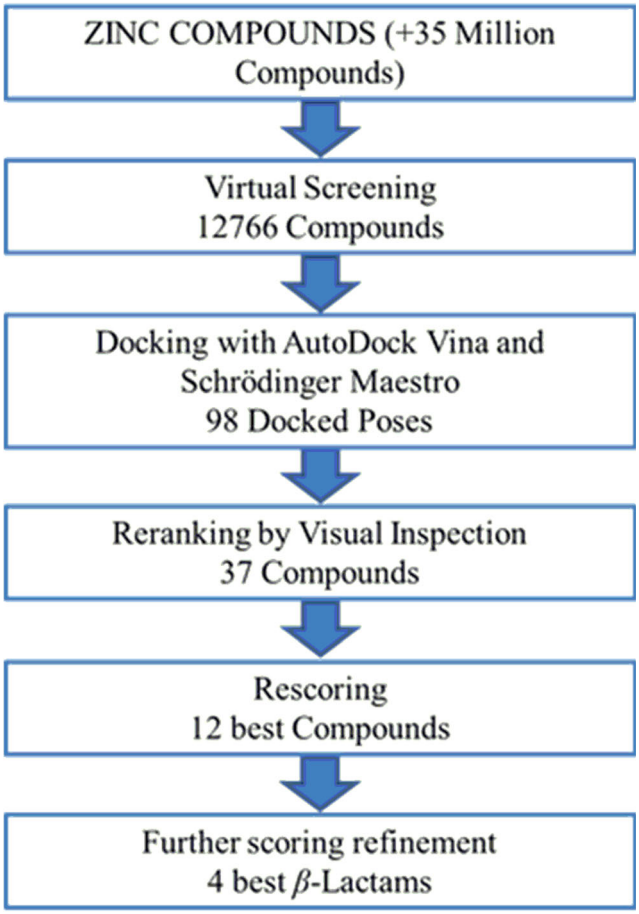

Fig. 2 Virtual screening workflow to the ten final lead compounds and further elucidation on four most potent β-lactams

randomized information exchange permitting exploration of the search space [26]. However, both software modules (Glide and AutoDock) identify multiple top-ranked docked poses per ligand. They both use hierarchical algorithms that are an exhaustive systematic search for the best ligand conformations within the protein active site; therefore, visual inspection for one best conformation per ligand, based on known interactions, was performed to identify a single best conformation per ligand for MD simulations.

Molecular dynamics simulation

MD simulations were performed to investigate the stability and dynamics of the complexes using the AMBER 14 package on GPUs with 24 shared processors using CHPC cluster. The ff99SB [49] force field and the general AMBER force field (GAFF) [50] were utilized to describe the protein and ligands, respectively. System solvation for the complexes was performed in a 10-Å cubic box by using the TIP3P water model. To neutralize the system negative value, sodium ions were added accordingly. The protein-ligand complexes were parametrized by the Leap [50] module of Amber 14 package. All simulations were performed using a 2-fs timestep (based on a study with similar protein size) and the rest of the process was also based on the same study [32]. The Particle Mesh Ewald (PME) [51] summation method was used to calculate the electrostatic forces with space cut-off of 12 Å. Using the SHAKE algorithm [52], all bonds were constrained to hydrogen (H) atoms. A two-stage energy minimization process, which is characterized by 2500 steps of steepest decent minimization and 2500 steps of conjugated gradient, was carried out to get rid of steric clashes. The solute molecule was first restrained at 500 kcal mol^{-1} whereas the water molecules and the ions were relaxed. The harmonic restraint was removed on the second stage; thus, the whole system was relaxed. Heating of the system to a constant temperature of 300 K was followed with a restraint of 10 kcal mol^{-1} for 200 ps, to keep the solute fixed. Density equilibration for 50 ps was performed and MD simulations ran at a constant temperature and pressure (1 atm). The Ldt_{Mt5}-ligand complexes ($n = 37$) were simulated for 50 ns [53]. The post-dynamics trajectory analysis including radius of gyration (Rg) and root mean square deviation (RMSD) was evaluated on the top 4 β-lactams with ≥ 30 kcal/mol. In addition to that, MD simulations (**Fig. S1**) were also performed in triplicate with different starting structures (varying initial atomic coordinates and velocities) [32, 54, 55] to validate the simulations.

Binding free energy calculation

MM-GBSA is a widely accepted method to compare the binding affinities and to gain rational insights about inhibitors by analysing the binding mechanism [56]. The average binding free energies (ΔG_{bind}) of the protein-ligand complexes were calculated for the last 10 ns using the MM-GBSA method [57]. Counter ions and water molecules were removed. Entropy penalty ($-T\Delta S$) for the complexes was obtained using normal mode analysis (nmode). The PTRAJ and CPPTRAJ modules [27] were used to analyse the MD trajectories.

Results and discussion

Data set preparation

A total of 12,766 antibacterial lead compounds in five categories listed in Table 2 were derived from ZINC database and were screened.

Table 5 Binding free energies and their corresponding components for compounds against Ldt_{Mt5} screened by AutoDock Vina using the AMBER 14 package. The docked 3D structures (PDB format) for all the lead compounds in complex with Ldt_{Mt5} are provided as supplementary information

ZINC ID	ΔE_{vdw}	ΔE_{ele}	ΔG_{gas}	ΔG_{polar}	$\Delta G_{non\text{-}polar}$	$\Delta G_{solvation}$	$-T\Delta S$	ΔG_{bind}
β-lactam								
02475683	*− 62.39*	*− 13.86*	*− 76.26*	*33.30*	*− 7.17*	*26.13*	*− 15.32*	*− 50.12*
02462884	*− 55.23*	*− 6.56*	*− 61.79*	*20.95*	*− 6.37*	*14.58*	*− 22.80*	*− 47.21*
03791246	− 28.02	− 139.32	111.30	− 126.03	− 3.53	− 129.56	− 15.97	− 18.26
Rifamycin								
14693083	*− 43.81*	*− 9.19*	*− 53.00*	*26.13*	*− 4.02*	*22.11*	*− 12.88*	*− 30.89*
13125731	− 32.74	− 8.25	− 40.99	21.78	− 3.29	18.50	− 14.19	− 22.50
13125732	− 28.82	− 4.69	− 33.50	18.10	− 2.92	15.18	− 16.11	− 18.32
Oxazolidinone								
00003190	− 36.88	− 2.95	− 39.82	14.31	− 4.19	10.12	− 21.83	− 29.71
05774946	− 27.29	− 3.30	− 30.59	11.56	− 3.55	8.00	− 17.04	− 22.58
00594969	− 18.28	− 1.02	− 19.30	8.48	− 2.25	6.23	− 19.08	− 13.07
Diarylquinoline								
00022456	*− 49.94*	*− 6.26*	*− 56.20*	*15.94*	*− 5.44*	*10.50*	*− 20.66*	*− 45.70*
00022457	*− 48.58*	*− 9.79*	*− 58.37*	*22.60*	*− 5.36*	*17.24*	*− 7.89*	*− 41.13*
00192295	− 34.01	− 2.33	− 36.35	14.32	− 3.21	11.10	− 14.01	− 25.25
Quinolone								
79236395	− 18.16	− 134.36	− 152.50	143.18	− 2.05	141.13	− 19.58	− 11.38
78317542	− 20.75	− 274.87	− 295.61	287.88	− 2.59	285.30	− 24.24	− 10.31

Compounds in italics are the best binders within the − 30 kcal mol^{-1} ≤ screening threshold and compounds in normal text are below the threshold

Ligand-based virtual screening and docking

Structural parameters were set to filter the compounds for screening based on Lipinski's rule-of-five (Table 1). Virtual screening of ligands was performed on a set of 98 docked poses and then considered for further visual inspection of the interaction [14] to determine the optimal ligand conformation per compound in the active pocket of Ldt_{Mt5}. A total of 46 top-ranked poses were obtained using AutoDock Vina (Table 3**)** and 52 from Schrödinger Maestro (Table 4). From there, a total of 37 compounds (13 from AutoDock Vina, Table 3 and 24 from Schrödinger Maestro Table 4) were selected for MD simulations and binding free energy calculations. Twelve out of the 37 compounds showed favourable binding energies greater than 30.0 kcal/mol. Further MD analysis was then carried out on the most potent 4 *β*-lactams with the binding free energies of ≥ 30.0 kcal/mol. Figure 2 shows the virtual screening workflow down to identify the final 4 potential *β*-lactam compounds.

The docking (consensus) scores for AutoDock Vina of the 10 top-ranked compounds across all classes lie between − 7.4 and − 9.0 kcal mol^{-1} (Table 3). The Schrödinger Maestro top-ranked docking scores were also considered, and the values are between − 7.2 and − 9.9 kcal mol^{-1} (Table 4). The docking scores of both software programs seem to be within the same range and both software programs optimize the ligand conformation during docking.

Binding free energy analysis

Our group has reported that MD studies provide comparable binding free energies for Ldt_{Mt2} with several inhibitors [32] to experiment. Based on the calculated docking scores, the complexes showing the best score and best ligand conformations within the protein active site were subjected to further molecular dynamics simulations using the AMBER 14 package. Similar protocol was carried out by John et al. and Islam et al. [53, 58]. With a cut-off-predicted binding energy (ΔG_{bind}) of ≤ − 30 kcal mol^{-1}, a final set of lead compounds ($n = 12$) (marked in bold) from four antibiotic classes was selected from Tables 5 and 6.

Two different classes of compounds were obtained as the best binders from utilizing the two docking programs. AutoDock Vina identified two lead compounds in terms of highest binding, both monobactams and these compounds showed greater predicted binding energies compared to the three carbapenems which were identified using Schrödinger Maestro (Table 7). The percentage of molecules saved during HTVS, SP Docking, XP Docking output respectively for each class of compounds is presented in Table S2.

The final set of compounds ($n = 12$) had all parameters within Lipinski's and Veber's constraints of drug-likeness (Table 8). It is noteworthy that all the screened compounds revealed a topological polar surface area (tPSA) > 150 $Å^2$, which is an indication of a high bioavailability [59].

Table 6 Binding free energies and their corresponding components for compounds screened by Schrödinger Maestro using the AMBER 14 package. The docked 3D structures (PDB format) for all the lead compounds in complex with Ldt_{Mt5} are provided as supplementary information

ZINC ID	ΔE_{vdw}	ΔE_{ele}	ΔG_{gas}	ΔG_{polar}	$\Delta G_{non\text{-}polar}$	$\Delta G_{solvation}$	$-T\Delta S$	ΔG_{bind}
β-lactam								
03784242	− 26.42	− 124.13	− 150.55	132.76	− 3.62	129.15	− 21.56	− 21.41
03785029	− 22.24	− 154.94	− 177.18	162.34	− 3.41	158.92	− 13.59	− 18.26
03785344	− 25.05	− 389.20	− 414.24	398.98	− 3.82	395.16	− 25.02	− 19.08
03785001	− 22.02	− 151.36	− 173.38	156.78	− 3.39	153.39	− 24.42	− 19.99
03808350	− 26.82	− 135.48	− 162.30	148.03	− 4.20	143.82	− 18.20	− 18.47
03808351	*− 36.95*	*− 199.77*	*− 236.72*	*197.99*	*− 4.93*	*193.06*	*− 20.83*	*− 43.66*
03808352	*− 34.19*	*− 181.75*	*− 215.93*	*186.83*	*− 5.20*	*181.63*	*− 27.31*	*− 34.31*
03826440	− 17.00	− 187.78	− 204.77	185.99	− 3.22	182.77	− 22.75	− 22.00
Rifamycin								
06483423	*− 38.83*	*− 13.74*	*− 52.57*	*26.44*	*− 4.38*	*22.06*	*− 18.46*	*− 30.51*
06483425	*− 43.36*	*− 4.38*	*− 47.74*	*16.48*	*− 5.23*	*11.24*	*− 15.33*	*− 36.50*
13532137	*− 43.36*	*− 11.64*	*− 55.00*	*25.37*	*− 5.23*	*20.14*	*− 18.39*	*− 34.87*
59077219	− 10.14	− 46.00	− 56.16	50.52	− 1.82	48.70	− 15.97	− 7.45
59077220	− 14.16	− 159.16	− 173.34	164.83	− 2.77	162.07	− 22.80	− 11.27
59077221	− 18.66	− 94.97	− 113.65	103.45	− 3.24	100.20	− 21.54	− 13.44
59077222	− 14.33	− 188.31	− 202.66	177.90	− 2.59	175.31	− 24.29	− 27.35
Oxazolidinone								
00052567	− 27.59	− 315.93	− 343.52	325.15	− 4.13	321.02	− 14.91	− 22.50
00052568	− 29.90	− 316.17	− 346.06	323.26	− 3.99	319.27	− 17.54	− 26.79
00108966	− 24.67	− 3.59	− 28.26	12.19	− 3.10	9.09	− 19.08	− 19.17
00108973	*− 41.00*	*− 2.10*	*− 43.10*	*11.79*	*− 4.67*	*7.11*	*− 10.25*	*− 35.98*
02512954	− 24.83	− 286.16	− 310.99	294.22	− 3.88	290.34	− 17.38	− 20.65
Diarylquinoline								
00002447	*− 44.25*	*− 262.29*	*− 306.55*	*277.55*	*− 5.66*	*271.89*	*− 14.10*	*− 34.65*
00007109	− 30.08	− 5.67	− 35.75	14.03	− 3.46	10.57	− 12.81	− 25.18
00060410	− 28.62	− 4.15	− 32.78	11.46	− 3.64	7.83	− 11.78	− 24.95
00096619	− 31.93	− 6.65	− 38.57	16.66	− 3.95	12.71	− 16.85	− 25.86

Compounds in italics are the best binders within the − 30 kcal mol^{-1} ≤ screening threshold and compounds in normal text are below the threshold

In light of the experimentally reported covalently bound interactions between L,D-transpeptidases and *β*-lactams, the subsequent section of this study focuses on better understanding of the binding interactions between the *β*-lactam class and Ldt_{Mt5}. To validate the virtual screening ranking and to compare the binding affinities, selected carbapenems known to inhibit Ldt_{Mt2} were screened for both Ldt_{Mt2} and Ldt_{Mt5} (Table 9). According to the consistent trend observed in Table 9 in terms of binding energies, the docking scores obtained seem to be valid.

Trajectory analyses of *β*-lactam-Ldt_{Mt5} complexes

Root mean square deviation analysis

RMSD is a measure of accuracy, comparing the differences between predicted values and observed values of a model [62]. The average values of the *β*-lactam-Ldt_{Mt5} complexes (A–D) (Fig. 3) are 1.91, 1.44, 1.40, and 1.25 Å respectively which lies in the accepted range of < 2.5 Å [14] for stable simulation.

The RMSD of the protein backbone and that of the ligand are presented in Figs. S2 and S3 respectively. In particular, a small and steady evolution of the ligand RMSD plot shows the stability of the ligands in the active sites during the simulation time.

Analysis of the radius of gyration

The radius of gyration is defined as the moment of inertia of the C-*α* atoms from its center of mass and it is used as an indicator of structural compactness of the protein-ligand complex [63, 64]. Figure 4 shows the Rg plots for the *β*-lactam-

Table7 Identified lead compounds with their antibacterial class, ZINC ID, calculated binding energies and the corresponding chemical structure, twelve in total. The docked 3D structures (PDB format) for all the lead compounds in complex with Ldt_{Mt5} are provided as supplementary information

Class	ZINC ID	ΔG_{bind} (kcal mol^{-1})	Structure
β-lactam	**02475683**	**-50.12**	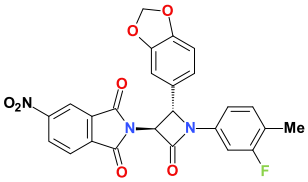
	02462884	**-47.21**	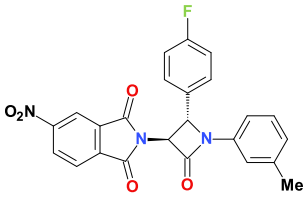
	03808351	-43.66	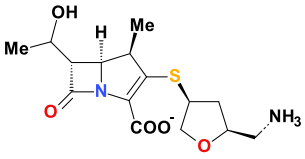
	03808352	-34.31	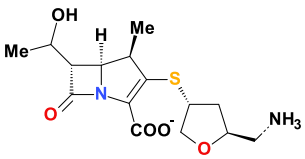
Diarylquinolone	**00022456**	**-45.70**	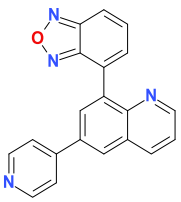
	00022457	**-41.13**	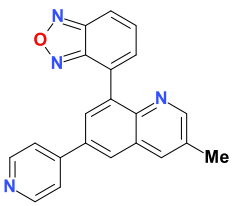

	00002447	-34.65	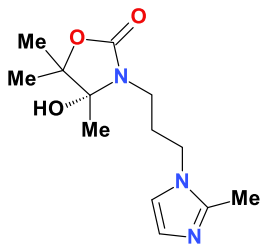
Oxazolidinone	00108973	-35.98	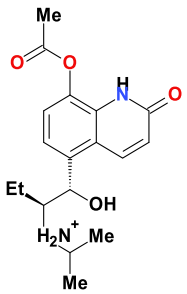
Rifamycin	06483423	-30.51	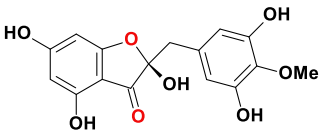
	06483425	-36.50	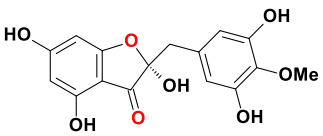
	13532137	-34.87	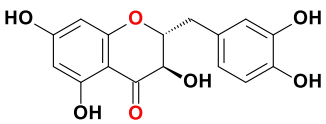
	14693083	**-30.89**	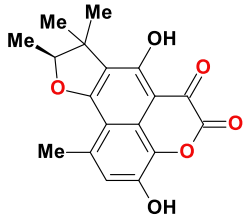

Compounds in bold were screened by AutoDock Vina [24] and compounds in normal text were screened by Schrödinger Maestro [25]

Table 8 Drug-like properties of the 12 potential leads from the ZINC database

ZINC ID	xlogP	Apolar desolvation (kcal mol^{-1})	Polar desolvation (kcal mol^{-1})	H bond donors	H bond acceptors	Net charge	tPSA (Å^2)	Molecular weight (g mol^{-1})	Rotatable bonds
**02475683*	4.37	11.33	− 14.54	0	10	0	124	489.415	4
**02462884*	4.53	12.58	− 14.66	0	8	0	105	445.406	4
*03808351	− 0.76	− 8.64	− 92.33	4	7	0	117	342.417	5
*03808352	− 0.76	− 8.61	− 86.43	4	7	0	117	342.417	5
¬00022456	4.06	1.31	− 14.65	0	5	0	64	324.343	2
¬00022457	4.49	1.62	− 14.46	0	5	0	64	338.37	2
00108973	0.69	− 1.15	− 18.45	1	6	0	67	267.329	4
00002447	1.43	− 1.02	− 53.74	4	6	1	96	333.408	7
06483423	0.98	− 7.89	− 15.73	5	8	0	136	334.28	3
06483425	0.98	− 7.88	− 15.31	5	8	0	136	334.28	3
13532137	0.92	− 3.03	− 13.32	5	7	0	127	318.281	2
14693083	3.22	5.51	− 13.4	2	6	0	97	328.32	0

Compounds in italics were screened by AutoDock Vina and compounds in normal text were screened by Schrödinger Maestro

*β-lactam

¬ Diarylquinoline

Oxazolidinone

Rifamycin

Ldt_{Mt5} complexes over a 50ns trajectory. The average Rg values for complex A (02475683-Ldt_{Mt5}), B (02462884-Ldt_{Mt5}), C (03808351-Ldt_{Mt5}), and D (03808352-Ldt_{Mt5}) reveal great overall similarity. The values are 29.38, 29.48, 29.68, and 30.46 Å respectively.

Binding free energy (ΔG_{bind}) analysis of β-lactam-Ldt_{Mt5} complexes

In this study, the calculated binding energies of β-lactam derivatives (meropenem and imipenem) against Ldt_{Mt2} from previous studies [32, 55] were used to validate the selection of lead compounds which demonstrated the best binding affinity for Ldt_{Mt5}. We hereby calculated the binding free energies (ΔG_{bind}) of the selected β-lactam-Ldt_{Mt5} complexes using the MM-GBSA method by extracting 1000 snapshots at 10 ps interval from the last 10 ns production MD trajectories. The entropy (-TΔS) contributions were calculated using normal mode analysis [65, 66] by extracting 100 snapshots from the MD trajectories. The contributing binding components upon complexation, namely, ΔE_{vdw}, ΔE_{ele}, ΔG_{gas}, ΔG_{polar}, $\Delta G_{nonpolar}$, and $\Delta G_{solvation}$ are shown in Table 10. The results reveal binding free energies of − 50.12 kcal mol^{-1} and − 47.21 kcal mol^{-1} for complex A (02475683-Ldt_{Mt5}) and complex B (02462884-Ldt_{Mt5}) respectively. The binding free energies of complexes C (03808351-Ldt_{Mt5}) and D (03808352-Ldt_{Mt5}) are − 43.66 kcal mol^{-1} and − 34.31 kcal mol^{-1}. It was observed that compounds with a greater binding affinity (A and B) are characterized by a more negative van der Waals value and they are less electronegative as compared with the other compounds (C and D).

Table 9 Comparison of the calculated binding energies for carbapenems on Ldt_{Mt5} against the calculated and experimental [60, 61] binding energies for Ldt_{Mt2}

Carbapenem	Ldt_{Mt2} ΔG_{exp} (kcal mol^{-1})	Ldt_{Mt2} ΔG_{docked} (kcal mol^{-1})	Ldt_{Mt5} ΔG_{docked} (kcal mol^{-1})
Biapenem	− 9.0[60]	− 6.7	− 6.2
Imipenem	− 9.8[61]	− 6.5	− 5.5
Meropenem	− 8.2[61]	− 7.1	− 6.3
Tebipenem	− 9.4[60]	− 6.6	− 6.0

The ZINC IDs for biapenem, imipenem, meropenem, and tebipenem are 03784073, 03830927, 03808779, and 04072129 respectively

Residue-inhibitor interaction analysis

To further elucidate the possible intermolecular hydrogen bonding and electrostatic interactions between β-lactam-Ldt_{Mt5} complexes, we used the LigPlot program [67]. The active site of Ldt_{Mt5} is defined by four conserved residues [His287 (342), Thr302 (357), Asn303 (358), and Cys305 (360)] [4]. Figure 5 shows the schematic representations of core amino acid residue interaction modes between the β-lactam compounds (A–D) and Ldt_{Mt5}. It is important to note that the residue-inhibitor interaction of compound A with Ldt_{Mt5} demonstrates close hydrogen bond interaction between the ligand and two active site residues Asn303 (358)

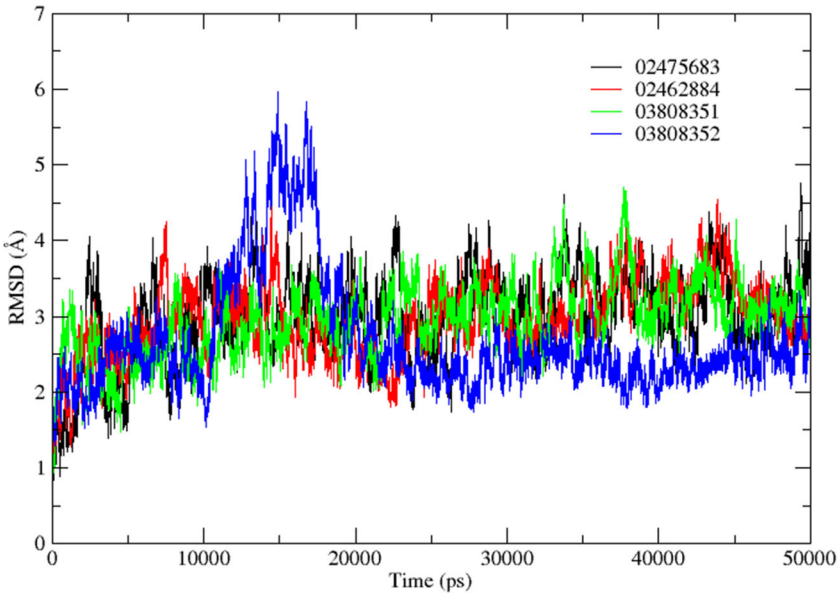

Fig. 3 Time evolution of the root mean square deviation (RMSD) of the β-lactam-Ldt_{Mt5} complexes of (A) 02475683-Ldt_{Mt5} (black), (B) 02462884-Ldt_{Mt5} (red), (C) 03808351-Ldt_{Mt5} (green), and (D) 03808352-Ldt_{Mt5} (blue) during 50ns MD trajectories. The docked 3D structures (PDB format) for all the lead compounds in complex with Ldt_{Mt5} are provided as supplementary information

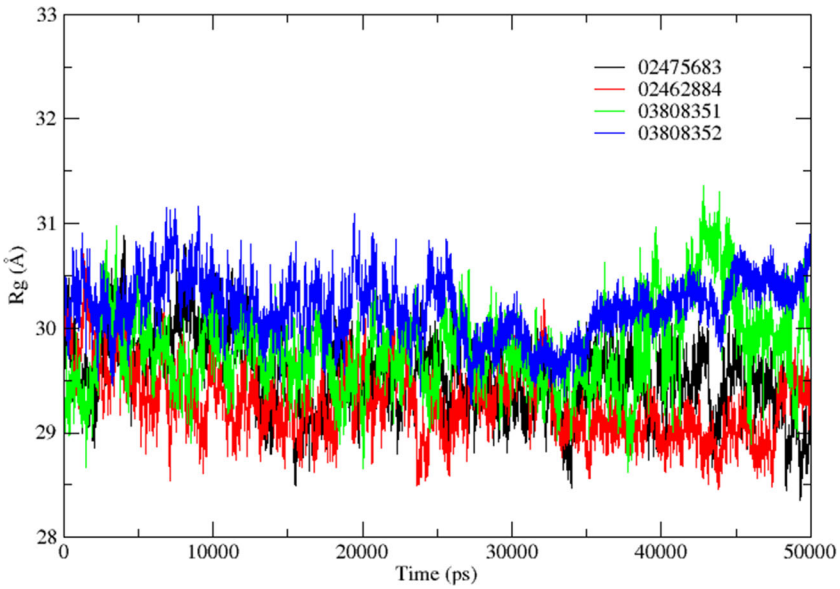

Fig. 4 The radius of gyration (Rg) of the β-lactam-Ldt_{Mt5} complexes of (A) 02475683-Ldt_{Mt5} (black), (B) 02462884-Ldt_{Mt5} (red), (C) 03808351-Ldt_{Mt5} (green), and (D) 03808352-Ldt_{Mt5} (blue) during 50-ns MD trajectories. The docked 3D structures (PDB format) for all the lead compounds in complex with Ldt_{Mt5} are provided as supplementary information

and Cys305 (360), which can be a possible explanation for the highest binding free energy observed. Compound B interacts with the residue Asn263 (318) and a water molecule which is within the active site (Fig. 5). The binding free energies (Table 10) of both compounds (A and B) are within the same range. Common between the other two compounds (C and D) is the interaction with residue Arg242 (297) and Gly304 (359). Compound C has other interactions with

Table 10 Calculated binding free energies and their corresponding components for the selected β-lactam-Ldt_{Mt5} complexes using the AMBER 14 package. The docked 3D structures (PDB format) for all the lead compounds in complex with Ldt_{Mt5} are provided as supplementary information

Compound	ZINC ID	ΔE_{vdw}	ΔE_{ele}	ΔG_{gas}	ΔG_{polar}	$\Delta G_{nonpolar}$	$\Delta G_{solvation}$	$-T\Delta S$	ΔG_{bind}
A	*02475683*	*− 61.93*	*− 14.22*	*− 76.16*	*33.47*	*− 7.14*	*26.34*	*− 15.32*	*− 50.12*
B	*02462884*	*− 55.30*	*− 6.57*	*− 61.88*	*20.97*	*− 6.36*	*14.61*	*− 15.97*	*− 47.21*
C	03808351	− 36.95	− 199.77	− 236.72	197.99	− 4.94	193.06	− 20.83	− 43.66
D	03808352	− 34.19	− 181.75	− 215.93	186.83	− 5.20	181.63	− 27.31	− 34.31

Compounds in italics were screened by AutoDock Vina and compounds in normal text were screened by Schrödinger Maestro

residues Glu284 (339), while compound D also interacts with Val244 (299) (Table 10). Both compounds are unique in that they interact with non-active site residues.

Results from virtual screening and docking studies demonstrated that several lead compounds from different classes of antibiotics potentially tend to bind to the active pocket of Ldt_{Mt5}. The binding free energies also demonstrate favourable binding potential of our lead compounds. It is known that β-lactams, specifically carbapenems, form covalent bonds with the catalytic cysteine (305) residue of Ldt_{Mt5} due to the carbonyl functional group in the structural backbone. However, results from the model as highlighted by the residue-inhibitor interaction analysis seem to suggest that other compounds may interact differently with Ldt_{Mt5}. Instead of forming covalent interactions, other potential inhibitors of Ldt_{Mt5} may perform competitive inhibition instead. It is also important to note that the closer the inhibitor interacts with the active site residues, the higher the binding affinity it may have, as

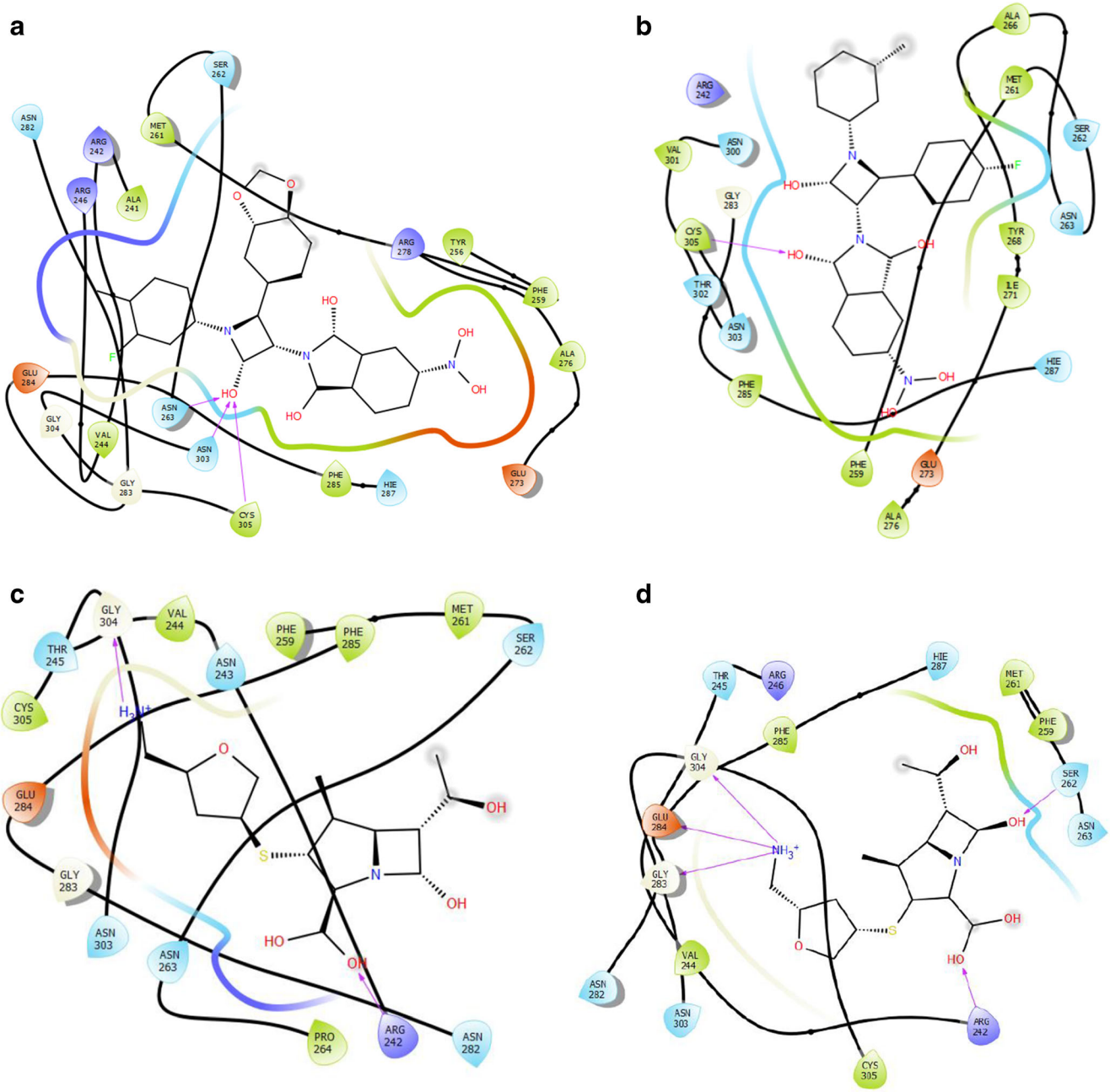

Fig. 5 2D schematic representations of the hydrogen bond interactions between Ldt_{Mt5} residues and the selected β-lactam compounds, ZINC ID (A) 02475683, (B) 02462884, (C) 03808351, and (D) 03808352. All structures are average conformations generated from the last 10-ns snapshots of each MD system

demonstrated by compound A (Fig. 5). This is also supported with the per-residue decomposition energy obtained through MM-GBSA calculations showing interactions with binding residues and some other important residues reported experimentally [4] (Fig. S4).

Conclusions

In this study, virtual screening of compounds from the ZINC database against Ldt_{Mt5} was investigated with AutoDock Vina and Schrödinger Maestro software programs. The obtained docking scores presented a reasonable number of lead compounds which can be utilized as potential drug candidates against Ldt_{Mt5}. Despite the lack of overlap on the screened compounds using these two different software programs, both provided reasonable binding scores. The observed exclusiveness of each program to a certain class of compounds strongly suggests that the effectiveness of a computational technique is subject to the software program utilized. To improve the chances of getting a "lead compound", different programs with alternative search algorithms need to be employed for the screening of compound libraries. It is essential to verify virtual screening results with MD free energy calculations as was demonstrated before [14]. The screened lead compounds were subjected to the MM-GBSA approach. A set of compounds ($n = 12$) from four antibiotic classes with ≤ -30 kcal mol^{-1} was obtained.

The computational model presented in this study is robust in that its accuracy was validated at both the docking stage as well as the MD simulation stage. Such benchmarking offers baseline comparisons of experimental and computational data from a paralog of the enzyme under study which brings about comparable extrapolations applicable to the natural system. The model as expressed through the docking affinities and binding energy calculations from MD simulations, demonstrated strong binding ligands. It should also be noted, however, that the residue-inhibitor interaction analysis further revealed that apart from the already known interactions, other compounds interact with other active site residues of the target. This certainly paves the way to explore other β-lactam binding mechanisms and expresses the importance of molecular dynamics simulations in revealing other possible interactions within the active site of other transpeptidases. We therefore conclude that pharmacophore-based virtual screening and molecular dynamics simulations are essential tools which will continue to play a significant role in drug design and identification of novel ligands.

Funding information Our gratitude goes to Aspen Pharmacare, National Research Foundation (NRF), and the University of KwaZulu-Natal (UKZN) for the financial support.

Compliance with ethical standards

Conflict of interest The authors declare that they have no conflict of interest.

References

1. Seung KJ, Keshavjee S, Rich ML (2015) Multidrug-resistant tuberculosis and extensively drug-resistant tuberculosis. Cold Spring Harbor perspectives in medicine:a017863
2. Billones JB, Carrillo MCO, Organo VG, Macalino SJY, Sy JBA, Emnacen IA, Clavio NAB, Concepcion GP (2016) Toward antituberculosis drugs: in silico screening of synthetic compounds against Mycobacterium tuberculosis L, D-transpeptidase 2. Drug Des Devel Ther 10:1147
3. Adewumi OA (2012) Treatment outcomes in patients infected with multidrug resistant tuberculosis and in patients with multidrug resistant tuberculosis coinfected with human immunodeficiency virus at Brewelskloof Hospital
4. Basta LAB, Ghosh A, Pan Y, Jakoncic J, Lloyd EP, Townsend CA, Lamichhane G, Bianchet MA (2015) Loss of a functionally and structurally distinct ld-transpeptidase, LdtMt5, compromises cell wall integrity in mycobacterium tuberculosis. J Biol Chem 290(42):25670–25685
5. Lavollay M, Arthur M, Fourgeaud M, Dubost L, Marie A, Veziris N, Blanot D, Gutmann L, Mainardi J-L (2008) The peptidoglycan of stationary-phase Mycobacterium tuberculosis predominantly contains cross-links generated by L, D-transpeptidation. J Bacteriol 190(12):4360–4366
6. Dubée V, Triboulet S, Mainardi J-L, Ethève-Quelquejeu M, Gutmann L, Marie A, Dubost L, Hugonnet J-E, Arthur M (2012) Inactivation of mycobacterium tuberculosis L, D-transpeptidase LdtMt1 by carbapenems and cephalosporins. Antimicrob Agents Chemother 56(8):4189–4195
7. Cordillot M, Dubée V, Triboulet S, Dubost L, Marie A, Hugonnet J-E, Arthur M, Mainardi J-L (2013) In vitro cross-linking of Mycobacterium tuberculosis peptidoglycan by l, d-transpeptidases and inactivation of these enzymes by carbapenems. Antimicrob Agents Chemother 57(12):5940–5945
8. Lecoq L, Dubée V, Sb T, Bougault C, Hugonnet J-E, Arthur M, Simorre J-P (2013) Structure of enterococcus faecium L, D-transpeptidase acylated by ertapenem provides insight into the inactivation mechanism. ACS Chem Biol 8(6):1140–1146
9. Gupta R, Lavollay M, Mainardi J-L, Arthur M, Bishai WR, Lamichhane G (2010) The mycobacterium tuberculosis protein LdtMt2 is a nonclassical transpeptidase required for virulence and resistance to amoxicillin. Nat Med 16(4):466–469
10. Biarrotte-Sorin S, Hugonnet J-E, Delfosse V, Mainardi J-L, Gutmann L, Arthur M, Mayer C (2006) Crystal structure of a novel β-lactam-insensitive peptidoglycan transpeptidase. J Mol Biol 359(3):533–538
11. Mainardi J-L, Fourgeaud M, Hugonnet J-E, Dubost L, Brouard J-P, Ouazzani J, Rice LB, Gutmann L, Arthur M (2005) A novel peptidoglycan cross-linking enzyme for a β-lactam-resistant transpeptidation pathway. J Biol Chem 280(46):38146–38152
12. Mainardi J-L, Villet R, Bugg TD, Mayer C, Arthur M (2008) Evolution of peptidoglycan biosynthesis under the selective pressure of antibiotics in Gram-positive bacteria. FEMS Microbiol Rev 32(2):386–408
13. Tolufashe GF, Sabe VT, Ibeji CU, Ntombela T, Govender T, Maguire GE, Kruger HG, Lamichhane G, Honarparvar B (2019) Structure and function of L, D-and D, D-transpeptidase family enzymes from Mycobacterium tuberculosis. Curr Med Chem

14. Honarparvar B, Govender T, Maguire GE, Soliman ME, Kruger HG (2013) Integrated approach to structure-based enzymatic drug design: molecular modeling, spectroscopy, and experimental bioactivity. Chem Rev 114(1):493–537
15. Bradley J, Garau J, Lode H, Rolston K, Wilson S, Quinn J (1999) Carbapenems in clinical practice: a guide to their use in serious infection. Int J Antimicrob Agents 11(2):93–100
16. Paterson D (2000) Recommendation for treatment of severe infections caused by Enterobacteriaceae producing extended-spectrum β-lactamases (ESBLs). Clin Microbiol Infect 6(9):460–463
17. Paterson DL Serious infections caused by enteric gram-negative bacilli–mechanisms of antibiotic resistance and implications for therapy of gram-negative sepsis in the transplanted patient. In: Seminars in respiratory infections, 2002. vol 4. pp 260–264
18. Paterson DL, Bonomo RA (2005) Extended-spectrum β-lactamases: a clinical update. Clin Microbiol Rev 18(4):657–686
19. Torres JA, Villegas MV, Quinn JP (2007) Current concepts in antibiotic-resistant gram-negative bacteria. Expert Rev Anti-Infect Ther 5(5):833–843
20. Meletis G (2016) Carbapenem resistance: overview of the problem and future perspectives. Ther Adv Infect Dis 3(1):15–21
21. Kattan J, Villegas M, Quinn J (2008) New developments in carbapenems. Clin Microbiol Infect 14(12):1102–1111
22. El-Gamal MI, Brahim I, Hisham N, Aladdin R, Mohammed H, Bahaaeldin A (2017) Recent updates of carbapenem antibiotics. Eur J Med Chem 131:185–195
23. Tolufashe GF, Sabe VT, Ibeji CU, Lawal MM, Govender T, Maguire GE, Lamichhane G, Kruger HG, Honarparvar B (2019) Inhibition mechanism of L, D-transpeptidase 5 in presence of the β-lactams using ONIOM method. J Mol Graph Model 87:204–210
24. Trott O, Olson AJ (2010) AutoDock Vina: improving the speed and accuracy of docking with a new scoring function, efficient optimization, and multithreading. J Comput Chem 31(2):455–461
25. Schrödinger Release 2018–1: Maestro S, LLC, New York, NY, 2018
26. Reddy AS, Pati SP, Kumar PP, Pradeep H, Sastry GN (2007) Virtual screening in drug discovery-a computational perspective. Curr Protein Pept Sci 8(4):329–351
27. Roe DR, Cheatham III TE (2013) PTRAJ and CPPTRAJ: software for processing and analysis of molecular dynamics trajectory data. J Chem Theory Comput 9(7):3084–3095
28. Pearlman DA, Case DA, Caldwell JW, Ross WS, Cheatham III TE, DeBolt S, Ferguson D, Seibel G, Kollman P (1995) AMBER, a package of computer programs for applying molecular mechanics, normal mode analysis, molecular dynamics and free energy calculations to simulate the structural and energetic properties of molecules. Comput Phys Commun 91(1–3):1–41
29. Berman HM, Westbrook J, Feng Z, Gilliland G, Bhat TN, Weissig H, Shindyalov IN, Bourne PE (2006) The protein data bank, 1999–. In: International tables for crystallography Volume F: Crystallography of biological macromolecules. Springer, pp 675–684
30. Sali A (1994) Modeller. A program for protein structure modeling by satisfaction of spatial restraints. http://guitar.rockefeller.edu/modiller/modeller.html
31. Li H, Robertson AD, Jensen JH (2005) Very fast empirical prediction and rationalization of protein pKa values. Proteins 61(4):704–721
32. Fakhar Z, Govender T, Maguire GE, Lamichhane G, Walker RC, Kruger HG, Honarparvar B (2017) Differential flap dynamics in l, d-transpeptidase2 from mycobacterium tuberculosis revealed by molecular dynamics. Mol BioSyst 13(6):1223–1234
33. Irwin JJ, Sterling T, Mysinger MM, Bolstad ES, Coleman RG (2012) ZINC: a free tool to discover chemistry for biology. J Chem Inf Model 52(7):1757–1768
34. Lipinski CA, Lombardo F, Dominy BW, Feeney PJ (2001) Experimental and computational approaches to estimate solubility and permeability in drug discovery and development settings1. Adv Drug Deliv Rev 46(1–3):3–26
35. Veber DF, Johnson SR, Cheng H-Y, Smith BR, Ward KW, Kopple KD (2002) Molecular properties that influence the oral bioavailability of drug candidates. J Med Chem 45(12):2615–2623
36. Singh UC, Kollman PA (1984) An approach to computing electrostatic charges for molecules. J Comput Chem 5(2):129–145
37. Gasteiger J, Marsili M (1980) Iterative partial equalization of orbital electronegativity—a rapid access to atomic charges. Tetrahedron 36(22):3219–3228
38. Morris GM, Huey R, Lindstrom W, Sanner MF, Belew RK, Goodsell DS, Olson AJ (2009) AutoDock4 and AutoDockTools4: automated docking with selective receptor flexibility. J Comput Chem 30(16):2785–2791
39. BIOVIA DS (2017) BIOVIA Discovery Studio 2017 R2: A comprehensive predictive science application for the Life Sciences. San Diego, CA, USA http://accelrys.com/products/collaborative-science/biovia-discovery-studio
40. Sastry GM, Adzhigirey M, Day T, Annabhimoju R, Sherman W (2013) Protein and ligand preparation: parameters, protocols, and influence on virtual screening enrichments. J Comput Aided Mol Des 27(3):221–234
41. Shelley JC, Cholleti A, Frye LL, Greenwood JR, Timlin MR, Uchimaya M (2007) Epik: a software program for pK a prediction and protonation state generation for drug-like molecules. J Comput Aided Mol Des 21(12):681–691
42. Harder E, Damm W, Maple J, Wu C, Reboul M, Xiang JY, Wang L, Lupyan D, Dahlgren MK, Knight JL (2015) OPLS3: a force field providing broad coverage of drug-like small molecules and proteins. J Chem Theory Comput 12(1):281–296
43. Jones G, Willett P, Glen RC, Leach AR, Taylor R (1997) Development and validation of a genetic algorithm for flexible docking. J Mol Biol 267(3):727–748
44. Friesner RA, Murphy RB, Repasky MP, Frye LL, Greenwood JR, Halgren TA, Sanschagrin PC, Mainz DT (2006) Extra precision glide: docking and scoring incorporating a model of hydrophobic enclosure for protein− ligand complexes. J Med Chem 49(21):6177–6196
45. Enyedy IJ, Egan WJ (2008) Can we use docking and scoring for hit-to-lead optimization? J Comput Aided Mol Des 22(3–4):161–168
46. Repasky MP, Shelley M, Friesner RA (2007) Flexible ligand docking with glide. Current protocols in bioinformatics:8.12. 11-18.12. 36
47. Metropolis N, Rosenbluth AW, Rosenbluth MN, Teller AH, Teller E (1953) Equation of state calculations by fast computing machines. J Chem Phys 21(6):1087–1092
48. Taylor RD, Jewsbury PJ, Essex JW (2002) A review of protein-small molecule docking methods. J Comput Aided Mol Des 16(3):151–166
49. Hornak V, Abel R, Okur A, Strockbine B, Roitberg A, Simmerling C (2006) Comparison of multiple Amber force fields and development of improved protein backbone parameters. Proteins 65(3):712–725
50. Wang J, Wolf RM, Caldwell JW, Kollman PA, Case DA (2004) Development and testing of a general amber force field. J Comput Chem 25(9):1157–1174
51. Harvey M, De Fabritiis G (2009) An implementation of the smooth particle mesh Ewald method on GPU hardware. J Chem Theory Comput 5(9):2371–2377
52. Kräutler V, Van Gunsteren WF, Hünenberger PH (2001) A fast SHAKE algorithm to solve distance constraint equations for small molecules in molecular dynamics simulations. J Comput Chem 22(5):501–508

53. John A, Sivashanmugam M, Umashankar V, Natarajan SK (2017) Virtual screening, molecular dynamics, and binding free energy calculations on human carbonic anhydrase IX catalytic domain for deciphering potential leads. J Biomol Struct Dyn 35(10): 2155–2168
54. Tolufashe GF, Halder AK, Ibeji CU, Lawal MM, Ntombela T, Govender T, Maguire GE, Lamichhane G, Kruger HG, Honarparvar B (2018) Inhibition of mycobacterium tuberculosis L, D-transpeptidase 5 by carbapenems: MD and QM/MM mechanistic studies. ChemistrySelect 3(48):13603–13612
55. Silva JRA, Bishai WR, Govender T, Lamichhane G, Maguire GE, Kruger HG, Lameira J, Alves CN (2016) Targeting the cell wall of mycobacterium tuberculosis: a molecular modeling investigation of the interaction of imipenem and meropenem with L, D-transpeptidase 2. J Biomol Struct Dyn 34(2):304–317
56. Sun H, Li Y, Tian S, Xu L, Hou T (2014) Assessing the performance of MM/PBSA and MM/GBSA methods. 4. Accuracies of MM/PBSA and MM/GBSA methodologies evaluated by various simulation protocols using PDBbind data set. Phys Chem Chem Phys 16(31):16719–16729
57. Miller III BR, McGee Jr TD, Swails JM, Homeyer N, Gohlke H, Roitberg AE (2012) MMPBSA. py: an efficient program for end-state free energy calculations. J Chem Theory Comput 8(9):3314–3321
58. Islam MA, Pillay TS (2017) Identification of promising DNA GyrB inhibitors for tuberculosis using pharmacophore-based virtual screening, molecular docking and molecular dynamics studies. Chem Biol Drug Des 90(2):282–296
59. Martin YC (2005) A bioavailability score. J Med Chem 48(9): 3164–3170
60. Bianchet MA, Pan YH, Basta LAB, Saavedra H, Lloyd EP, Kumar P, Mattoo R, Townsend CA, Lamichhane G (2017) Structural insight into the inactivation of Mycobacterium tuberculosis non-classical transpeptidase Ldt Mt2 by biapenem and tebipenem. BMC Biochem 18(1):8
61. Erdemli SB, Gupta R, Bishai WR, Lamichhane G, Amzel LM, Bianchet MA (2012) Targeting the cell wall of mycobacterium tuberculosis: structure and mechanism of L, D-transpeptidase 2. Structure 20(12):2103–2115
62. Hyndman RJ, Koehler AB (2006) Another look at measures of forecast accuracy. Int J Forecast 22(4):679–688
63. Lobanov MY, Bogatyreva N, Galzitskaya O (2008) Radius of gyration as an indicator of protein structure compactness. Mol Biol 42(4):623–628
64. Peterson K, Zimmt M, Linse S, Domingue R, Fayer M (1987) Quantitative determination of the radius of gyration of poly (methyl methacrylate) in the amorphous solid state by time-resolved fluorescence depolarization measurements of excitation transport. Macromolecules 20(1):168–175
65. Kassem S, Ahmed M, El-Sheikh S, Barakat KH (2015) Entropy in bimolecular simulations: a comprehensive review of atomic fluctuations-based methods. J Mol Graph Model 62:105–117. https://doi.org/10.1016/j.jmgm.2015.09.010
66. Chiba S, Harano Y, Roth R, Kinoshita M, Sakurai M (2012) Evaluation of protein-ligand binding free energy focused on its entropic components. J Comput Chem 33(5):550–560. https://doi.org/10.1002/jcc.22891
67. Wallace AC, Laskowski RA, Thornton JM (1995) LIGPLOT: a program to generate schematic diagrams of protein-ligand interactions. Protein Eng Des Sel 8(2):127–134